Two-Dimensional Pigment Monolayer Assemblies for Light-Harvesting Applications: Structural Characterization at the Air/Water Interface with X-ray Specular Reflectivity and on Solid Substrates by Optical Absorption Spectroscopy

Brian W. Gregory,[†,‡] David Vaknin,[*,§] John D. Gray,[§] Ben M. Ocko,[⊥] Pieter Stroeve,[¶] Therese M. Cotton,[†] and Walter S. Struve[*,†]

Ames Laboratory-USDOE, Department of Chemistry, and Department of Physics and Astronomy, Iowa State University, Ames, Iowa 50011; Department of Physics, Brookhaven National Laboratory, Upton, New York 11973; and Department of Chemical Engineering, University of California—Davis, Davis, California 95616

Received: October 15, 1996; In Final Form: January 6, 1997[⊗]

X-ray specular reflectivity at the liquid/gas interface of dihexadecyl phosphate (DHDP) on pure H_2O and on a series of pigment-containing aqueous solutions are reported along with visible absorption spectra of corresponding monomolecular Langmuir−Blodgett films on quartz substrates. Molecular level interpretation of the reflectivity from DHDP on pure water reveals that at large surface pressure (>10 mN/m), the film is closely packed with practically untilted hydrocarbon chains and hydrated phosphate headgroups. On solutions containing either water-soluble cationic tetraazaphthalocyanines or tetrapyridylporphyrins, significant changes in the organization of the lipid with respect to that on pure water are found. Total film thicknesses are larger and consistent with the adsorption of a single pigment layer contiguous to the headgroup, whereas the hydrocarbon *tail* region is shorter, suggestive of tilted alkyl chains. In addition, film thicknesses for phthalocyanine-containing films suggest formation of an iodide counterion layer *underneath* the plane containing the pigments. This sharply contrasts the interfacial profile obtained for porphyrin-containing films, in which the iodide counterions appear to exist *within* the pigment plane. Visible absorption spectra of all transferred films indicate a closely packed single pigment layer, consistent with the reflectivity results. The optical spectra of the pigment are preserved (in relation to the aqueous solution monomer spectra) in the transferred film, indicating a suppression of pigment aggregation. Reflectivity measurements at large molecular areas on pure water indicate that DHDP forms an inhomogeneous film, suggestive of phase segregation; on the pigment-containing solutions, DHDP induces (through attractive Coulomb interactions) the adsorption of a homogeneous monopigment layer. The existence of a complete pigment monolayer over the measured surface pressure−molecular area ($\pi-A$) isotherms has been evidenced by both X-ray reflectivity and visible optical studies. Preservation of pigment functionality has been demonstrated through the process of Coulomb association of the chromophores with charged lipid monolayer headgroups at the air/water interface. The potential for applications as model photosynthetic antennae will be discussed.

1. Introduction

Activity in the synthesis of biomimetic supramolecular assemblies that replicate the light-harvesting and electronic energy transfer functions of natural photosynthetic antennae has greatly accelerated in recent years.[1−4] An effective antenna must present a large total cross section for light absorption per reaction center; reaction centers in natural photosynthetic units are typically associated with several tens to several thousands of antenna pigments.[5,6] For efficient singlet−singlet electronic energy transfer, the pigments must be closely spaced (nearest-neighbor separations <20−40 Å). The pigment fluorescing state must be connected to the ground state by a strongly dipole-allowed transition, because the rate constant for Förster energy transfer scales with $\int \epsilon_A(\omega) f_D(\omega) d\omega/\omega^4$; here $\epsilon_A(\omega)$ and $f_D(\omega)$ are the acceptor absorption spectrum and the normalized donor fluorescence spectrum, respectively.[7] The absorption cross sections for the strongest electronic transitions known in nature ($\epsilon_{max} \sim 10^5$ L/(mol·cm) for Chl *a* and BChl *a*) are somewhat smaller (~3.5 Å^2) than the physical pigment size.[8] The use of pigments with significantly smaller cross sections thus results in inefficient use of space. Many potential biomimetic pigments spontaneously also form nonfluorescing aggregates, which are unsuitable for antenna function. This is one of the most difficult challenges in designing artificial assemblies of pigments for light-harvesting purposes, and therefore methods which suppress their formation are highly desirable. Finally, the pigments and their support matrix must be thermally and photochemically durable.

Porphyrins are spectroscopically unfavorable for use in efficient antennae because their comparatively weak $S_0 \rightarrow S_1$ transitions[9] foster slow singlet energy transfers. Chlorins and bacteriochlorins (which include the bulk of natural photosynthetic pigments) are spectroscopically optimal for light harvesting and energy transfer, but they are thermally and photochemically unstable outside of their natural protein environments. Phthalocyanines exhibit intense $S_0 \rightarrow S_1$ transitions ($\epsilon_{max} \sim 10^5$ L/(mol·cm)), *and* they are exceptionally durable. While ph-

* Authors to whom correspondence should be addressed.
† Present address: Department of Chemistry, Illinois State University, Normal, IL 61790-4160.
‡ Ames Laboratory-USDOE and Department of Chemistry, Iowa State University.
§ Ames Laboratory−USDOE and Department of Physics and Astronomy, Iowa State University.
⊥ Brookhaven National Laboratory.
¶ University of California−Davis.
⊗ Abstract published in *Advance ACS Abstracts,* February 15, 1997.

S1089-5647(96)03152-5 CCC: $14.00

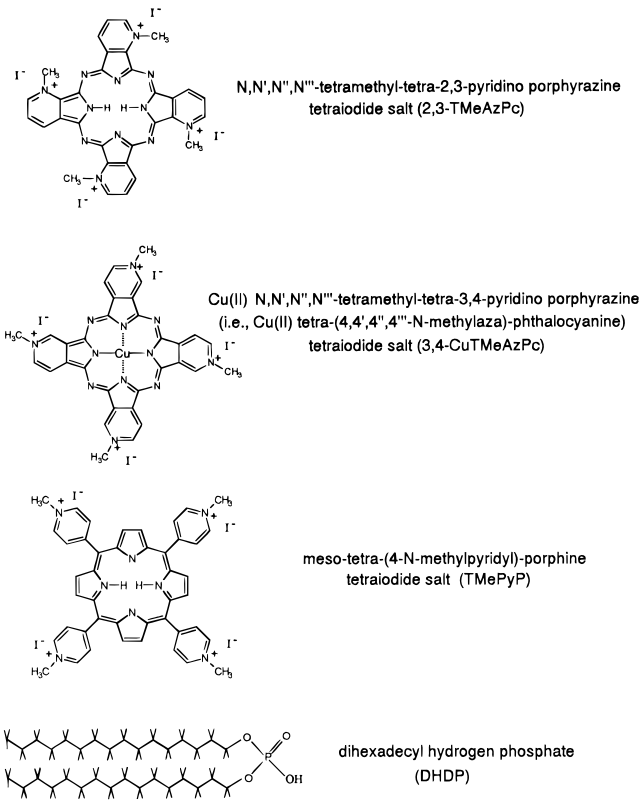

Figure 1. Chemical structures of the dialkyl phosphate and pigments used in these studies.

thalocyanines form an important class of industrial dyes,[10] they have been little used in artificial photosynthesis, perhaps because their chemistry (unlike that of porphyrins) is relatively undeveloped. For example, few stratagems have been developed for functionalizing them, or for binding them to protein residues.

In this work, we have constructed Langmuir films consisting of dialkyl phosphate monolayers (MLs) which interact Coulombically at the air/water (A/W) interface with charged, water-soluble tetraazaphthalocyanine pigments (Figure 1). These tetraazaphthalocyanines are isoelectronic with the corresponding phthalocyanines, and thus exhibit similar electronic selection rules (i.e., their intense $S_0 \rightarrow S_1$ transitions are closely analogous to those of the corresponding phthalocyanines). The chromophores are rendered water-soluble through quaternization with CH_3I, which yields the tetramethylated, tetracationic product (Figure 1).[11,12] The water-soluble tetraazaphthalocyanine does not spontaneously aggregate in aqueous solution, but remains monomeric.[11,12] In addition, its tendency to aggregate in the complexed state with the dialkyl phosphate at the A/W interface is overridden by the strong repulsive Coulomb interactions between neighboring positively charged macrocycles and by the favorable Coulomb interactions with the negatively charged dialkylphosphate headgroups. Similar interactions were exploited by Palacin and co-workers[13] in their synthesis of two-dimensional polymers from tetrapyridylporphyrins at the A/W interface. Thus, the resulting film ideally comprises both a lipid and pigment layer (Figure 2), where lipid and pigment surface densities are expected to be large, particularly at high surface pressurs (π). The notion that such interfacial complexation drives the formation of a homogeneous, unaggregated, coplanar array of porphine-based macrocycles, as enunciated in ref 13 and suggested in ref 14, has not been directly verified prior to this report.

In these studies, surface pressure−molecular area ($\pi-A$) isotherms and *in situ* X-ray specular reflectivity studies of our

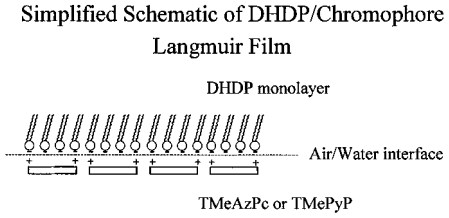

Figure 2. Generalized schematic showing interfacial complexation at air/water interface between negatively charged dialkyl phosphates and positively charged, water-soluble pigments.

monolayers were employed to determine the interfacial structures of these systems. Specular reflectivity of X-rays is sensitive to the electron density normal to the interface and therefore can probe the thickness of the pigment region *in situ* and yield information about chromophore organization. Determination of the interfacial structures in these dialkyl phosphate/pigment systems is accomplished by refining a slab model, with which the reflectivities are calculated using the Parratt recursive formalism.[15] The slab model, which depicts the interfacial electron density profile normal to the interface, facilitates the calculation by allowing one to partition the monolayer film into sections of uniform electron density (e.g., hydrocarbon tails, headgroups, etc.). Particular attention is directed toward a molecular-level description of the dialkyl phosphate monolayer itself (dihexadecyl hydrogen phosphate, DHDP), and its relationship to similar lipid monolayers (such as arachidic acid[16] and dipalmitoylphosphatidylcholine, DPPC[17]). The X-ray investigations reported here are more detailed than given in a preliminary analysis.[18] In addition, optical density and linear dichroism measurements of monolayer films transferred onto quartz substrates (i.e., Langmuir−Blodgett (LB) monolayers) have been performed in order to ascertain mean pigment surface densities and orientations, respectively. The optical densities for the $S_0 \rightarrow S_1$ absorption bands in our LB tetraazaphthalocyanine films correspond to nearest-neighbor pigment separations as low as 14−16 Å. The absorption bands in these films are not significantly changed either in shape (i.e., bandwidth) or position from those of the same pigment in dilute solution. Hence, LB film antennae have been successfully prepared with minimal aggregation. Similar measurements have also been made for comparison on aqueous solutions containing water-soluble *meso*-tetra-(4-*N*-methylpyridyl)porphyrins. Kinetic energy transfer studies of these Langmuir−Blodgett films will be reported in future work.

2. Experimental Section

2.1. Materials and Monolayer Preparation. Monolayers of dihexadecyl hydrogen phosphate (DHDP, Aldrich, 99%) (Figure 1) were prepared at a gas/liquid interface in a thermostated, solid Teflon Langmuir trough placed within a nitrogen-purged box. Aqueous solutions containing 1−2 μM *N,N′,N″,N‴*-tetramethyltetra-2,3-pyridinoporphyrazine, tetraiodide salt (i.e., tetra-(*N*-methylaza)phthalocyanine (2,3-TMeAzPc), Porphyrin Products, >97%) (Figure 1); "saturated" (<1 μM) copper(II) *N,N′,N″,N‴*-tetramethyltetra-3,4-pyridinoporphyrazine, tetraiodide salt (3,4-CuTMeAzPc, Aldrich (unquaternized reagent)) (Figure 1); or 1−2 μM 5,10,15,20-tetra-(4-*N*-methylpyridyl)-21*H*,23*H*-porphine, tetraiodide salt (TMePyP, Strem, 95%) (Figure 1) were used as the subphases in these experiments. Both lipid and pigments were used as received. (It should be mentioned here that the solubility of 3,4-CuTMeAzPc in aqueous solution at neutral pH is quite low; thus, the term "saturated" will be used to signify solutions which would have resulted in 1−2 μM 3,4-CuTMeAzPc concentrations if the

compound were completely soluble. Therefore, "saturated" signifies <1 μM 3,4-CuTMeAzPc.) Ultrapure water (Millipore Milli-Q, nominal resistivity = 18 MΩ cm) was used for all subphase preparations. The subphase temperature was maintained at 20 ±2 °C. The DHDP spreading solutions were prepared at 1−2 mM concentrations in $CHCl_3$ (Fisher, HPLC grade). After an appropriate volume of solution was spread on the subphase surface, a 15−20 min equilibration period was allowed for solvent evaporation before compression was begun. The monolayer was then compressed at a rate of ∼0.020−0.025 Å^2/(molecule·sec). Surface pressures were recorded by differential weight measurements using a filter paper Wilhelmy plate suspended from a linear variable differential transducer.

Transfer of DHDP and DHDP/pigment monolayers was accomplished via LB methodology.[19] Quartz slides (2 mm thick, ∼8 cm^2 surface area), which were extensively cleaned in $Na_2Cr_2O_7/H_2SO_4$ solutions just prior to deposition, were used for all transfers. Following immersion of the substrate in the subphase, the lipid monolayer was spread onto the subphase surface. After the 15−20 min equilibration period, the lipid monolayer was compressed (at the same rate as in the $\pi-A$ isotherms) to the desired final surface pressure or molecular area. After another 0.5 h period to allow for monolayer equilibration, the substrate was then raised vertically through the compressed monolayer film at 2 mm/min. The monolayer was deposited in a single pass through the A/W interface; measured transfer ratios were typically 1.0 ± 0.05. Although all LB transfers were performed at constant surface pressure ($\pi_{transfer}$), it should be noted, however, that some transfers were performed at very large molecular areas, where π's for some of these DHDP/pigment films are ∼0 mN/m. In these instances, depositions were accomplished by compressing the film to a predefined molecular area, disengaging barrier movement, and transferring the film with no change in the overall film area. All depositions performed in this manner exhibited no change in $\pi_{transfer}$ during the transfer process. In addition, the substrate surface areas were kept to <5% of the total film area to minimize drastic changes in the molecular area during this procedure. For DHDP/TMePyP monolayers, instability in the initial, as-spread film structure, evident from the $\pi-A$ isotherms (see section 3.1), was also reflected in some difficulty in performing monolayer depositions. Despite the fact that constant surface pressures could be maintained for all transfers attempted, constant and steady film areas could not be maintained prior to deposition for $\pi_{transfer}$'s < 10 mN/m. Once $\pi_{transfer}$ was attained in this surface pressure regime, cessation of barrier movement resulted in a gradual decrease in the surface pressure until π was approximately 0−1 mN/m. Thus, in order to maintain constant $\pi_{transfer}$'s prior to deposition for π < 10 mN/m, constant and steady compression of the monolayer (under control of the surface pressure feedback sensing circuit) was necessary and unavoidable. Transer ratios were therefore measured as the change in the rate of barrier movement during deposition.

Additional experiments were attempted in which DHDP/pigment monolayers were transferred by immersion (i.e., downstroke) of a hydrophobic, *n*-octadecylsilane-modified quartz substrate through the film at the A/W interface at high π into the subphase. After immersion, the subphase surface was thoroughly cleaned by aspirating the excess monolayer off. The substrate was subsequently raised through the clean subphase surface. Although immersion transfer of these DHDP/pigment monolayers was apparently accomplished on the downstroke (as verified by monitoring the change in film area), all pigments apparently dissociated from the surface upon removal from the subphase, since no visible optical spectra attributable to pigments could be obtained.

2.2. X-ray Specular Reflectivity. Reflectivity measurements of spread films were performed on a liquid-surface X-ray reflectometer constructed in-house and on the Harvard-Brookhaven Liquid spectrometer (X22B beamline) at the National Synchrotron Light Source (NSLS) at Brookhaven National Laboratory. The Ames Laboratory apparatus is similar to one described by Als-Nielsen and Pershan.[20] Both the Ames Laboratory and NSLS spectrometers have been described previously.[21,22] The NSLS spectrometer[22] (operating at λ = 1.583 Å) provides ∼1000 times greater flux than compared to those employing a rotating anode, and this permits measurements to be carried out to larger incident angles. Reflectivity measurements on all four monolayer systems were initially carried out on the spectrometer at the Ames Laboratory; the work on DHDP, DHDP/2,3-TMeAzPc, and DHDP/TMePyP was subsequently extended on the NSLS spectrometer. Due to their inherently higher sensitivity and quality, the NSLS data are presented herein, except for DHDP/3,4-CuTMeAzPc. Preliminary results have been published elsewhere.[18]

In X-ray specular reflectivity experiments, a monochromatic X-ray beam of intensity I_0 is incident upon a surface at an angle α_i, and the reflected beam intensity I_r is detected at an angle α_r under specular reflection conditions (i.e., $\alpha_i = \alpha_r$, where α_i and α_r are measured relative to the interfacial plane). The background at each angle is determined by measuring the diffuse intensity under off-specular conditions and is subtracted from the specularly reflected beam intensity. The reflectivity as a function of the momentum transfer, $Q_z = (4\pi/\lambda)\sin\alpha$, is defined as $R(Q_z) = I_r/I_0$. The refractive index of air for X-rays with wavelengths near 1 Å is unity and that of a homogeneous medium of electron density $\rho(z)$ is given by[23,24]

$$n(z) = 1 - (\lambda^2/2\pi)\rho(z)r_0 \qquad (1)$$

where r_0 is the classical radius of the electron ($r_0 = 2.82 \times 10^{-13}$ cm). For a single sharp discontinuity in the electron density between two media of different refractive indices, total external reflection occurs below a certain critical angle α_c, the value of which depends on the optical properties of the two media and the wavelength λ of the radiation ($\alpha_c = \lambda(\rho_{bulk}r_0/\pi)^{1/2}$ (ref 24)). Above α_c, the reflectivity falls of monotonically with increasing α (i.e., increasing Q_z) as $(\alpha_c/2\alpha_i)^4$.[24] The reflectivity at a single, ideally sharp interface is referred to as the Fresnel reflectivity $R_F(Q_z)$.[25] In the case of a stratified sample with sharp interfaces, multiple reflections occur at each interface, giving rise to interference between the different reflected beams.[24,25] These interference patterns appear as intensity modulations superimposed upon $R_F(Q_z)$. The reflectivity from a finite number of ideally sharp interfaces, $R_0(Q_z)$, can be exactly calculated using standard recursion methods.[15] In this approach, the electron density profile is constructed as the sum of N step functions, each representing regions of constant electron density. To account for interfacial roughness arising from thermal capillary wave motion and surface imperfections, and working under the assumption of Gaussian-smeared interfaces (i.e., convolution of step functions with a Gaussian of the form $\exp(-1/2(z - z_i/\sigma)^2)$), the reflectivity is modified by a Debye−Waller-like factor[24]

$$R(Q_z) = R_0(Q_z)e^{-(Q_z\sigma)^2} \qquad (2)$$

where σ, a roughness factor with units of length (Å), is a measure of the width of the interface between constant-density regions.[26]

A more insightful description of the relationship between the observed reflectivity and the electron density profile is given by the kinematical approximation[24,27]

$$R(Q_z) = R_F(Q_z)\left|\frac{1}{\rho_{bulk}}\int\left(\frac{d\rho}{dz}\right)e^{iQ_z z}\,dz\right|^2 \qquad (3)$$

where ρ_{bulk} and $R_F(Q_z)$ are the electron density and Fresnel reflectivity, respectively, of the pure aqueous subphase. Here the intensity modulations in $R(Q_z)$ are related to the Fourier transform of the electron density gradient along the direction normal to the interfacial plane. Thus, the experimental ratio $R(Q_z)/R_F(Q_z)$ reflects information specific to monolayer structure along the normal. It has been demonstrated[24] that both computational approaches, dynamical and kinematical, yield equivalent results for $Q_z > Q_c$; differences between the two arise for $Q_z \sim Q_c$ since multiple scattering effects have been ignored in the kinematical method.

2.3. Optical Spectroscopy. Electronic absorption spectra of transferred monomolecular DHDP/pigment films were obtained with a Perkin-Elmer Lambda 6 UV−vis spectrophotometer, operating at a scan rate of 200 nm/min with a slit width of 1.0 nm. Surface molecular densities were calculated from the measured optical densities of the 2,3-TMeAzPc $S_0 \rightarrow S_1$ transition (ϵ_{soln} (641 nm) = 98 000 L mol^{-1} cm^{-1} (ref 11)) and the TMePyP Soret band (ϵ_{soln} (421 nm) = 280 000 L mol^{-1} cm^{-1} (ref 28)). (A small correction factor was applied to the extracted surface densities in order to account for the anisotropic distribution of the pigment electronic transition moments within the film in comparison with isotropic solution values. Since the pigment tilt angles (obtained from electronic linear dichroism measurements, see below) are approximately 60°−70° (relative to the surface normal), the calculated pigment surface densities are approximately 20−30% lower than expected based on the solution extinction coefficients; thus, the molecular areas are approximately 20−30% larger.) Extraction of molecular surface densities for the DHDP/3,4-CuTMeAzPc films, however, was hampered by extremely low $S_0 \rightarrow S_1$ band intensities. This effect mirrored that observed in its aqueous solution-phase spectra, which indicated the presence of aggregation (in comparison with the monomeric spectra obtained in 1-chloronaphthalene; see section 3.3.2). Suitable control experiments for each pigment consisted essentially of an LB deposition in which no DHDP film was spread prior to transfer; these were performed in order to measure the amount of pigment which might (1) spontaneously adsorb to the quartz surface or (2) precipitate from the emersion layer upon removal from the pigment-containing subphase. In order to reproduce the original transfer conditions as closely as possible, the substrate was left immersed in the subphase for periods of time equivalent to that required for an actual LB transfer. All other deposition conditions were identical to those involving the DHDP film. Quantitation of the resulting pigment optical spectra from the substrates demonstrated that the total contribution of both processes was ∼5−8% of that observed with the corresponding DHDP/pigment monolayers. Thus, the DHDP/pigment monolayer optical spectra arise primarily from the transferred film and not from other sources.

In addition to optical density measurements, a substrate rotation stage (equivalent to that in ref 32) was designed for linear dichroism studies which allowed one to vary the angle between the plane of the film and the electric vectors of the incident radiation. Reference spectra were obtained from a clean quartz slide at the same angles. The theory of linear dichroism is well-known and has been applied extensively to the study of thin films.[29−34] The dichroic ratio P is commonly defined as

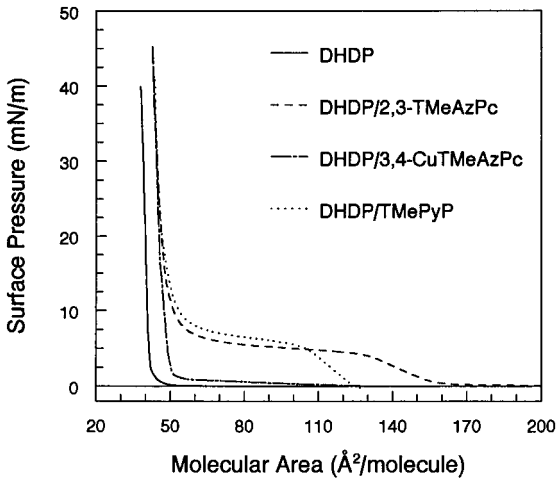

Figure 3. $\pi-A$ isotherms of DHDP on H_2O, 1 μM 2,3-TMeAzPc, saturated 3,4-CuTMeAzPc, and 1 μM TMePyP.

$$P = \int A_s\,d\lambda / \int A_p\,d\lambda \qquad (4)$$

where A_s and A_p correspond to the experimentally determined absorbances for s- and p-polarized radiation, respectively. (Equation 4 strictly holds only for samples in which the change in transmittance $\Delta T < 1\%$,[30] which for most monolayer films is reasonable.) For a uniaxially oriented sample, this ratio is related to the angle of incidence (α) of the impinging radiation and the average azimuthal orientation angle (θ) of the transition dipole (relative to the surface normal) through

$$P = (\cos^2\alpha + 2\sin^2\alpha\cot^2\theta)^{-1} \qquad (5)$$

Therefore, measurement of the dichroic ratio as a function of the angle of incidence allows one to calculate the average molecular orientation within the film.

3. Results and Discussion

3.1. Monolayer $\pi-A$ Isotherms. The $\pi-A$ isotherms of DHDP on pure H_2O, 1 μM 2,3-TMeAzPc, saturated 3,4-CuTMeAzPc, and 1 μM TMePyP are shown in Figure 3. Substantial differences are observed in the $\pi-A$ behavior for DHDP on these four different subphases. The limiting molecular area of DHDP on H_2O is approximately 41 ± 1 Å^2/molecule, which agrees well both with estimates from space-filling (i.e., Corey−Pauling−Koltun (CPK)) models and previously published studies.[13,35] The limiting molecular areas for DHDP/2,3-TMeAzPc, DHDP/3,4-CuTMeAzPc, and DHDP/TMePyP at high surface pressure are approximately 4−6 Å^2/molecule larger compared to DHDP on H_2O, suggesting that the lipid films are expanded due to their interaction with the interfacially bound pigments. (All molecular areas discussed in relation to the $\pi-A$ isotherms correspond solely to DHDP and not to the chromophores, since the area per lipid is the measured quantity. We recall that the system consists of two interacting layers which are not mutually covalently bound and that the pigment can exist in either the film or in the subphase; the lipid is confined to the A/W interface.) The comparability of these limiting areas suggests that the structure of the lipid film is similar at high surface pressure in all three chromophore systems. Although the limiting molecular area of DHDP on all three pigment-containing solutions converges to the same value (approximately 46 ± 2 Å^2/molecule), significant differences in the isotherms are noticeable at larger molecular areas.

The most noticeable difference between the three pigment-containing films at large molecular areas is the presence of a

TABLE 1: DHDP Monolayer Structure on Pure H_2O at $\pi = 40$ mN/m

independent Variables		
d_{tail} (Å)	19.7 ± 0.4	thickness of hydrocarbon tail layer
d_{head} (Å)	3.4 ± 0.8	thickness of phosphate headgroup layer
N_{H_2O}	3.2 ± 1.4	no. of H_2O's associated with headgroup
σ (Å)	3.22 ± 0.10	interfacial roughness
dependent Variables		
ρ_{tail} (e/Å^3)	0.319 ± 0.006	electron density of hydrocarbon tail layer
ρ_{head} (e/Å^3)	0.574 ± 0.250	electron density of headgroup layer
θ (deg)	7 ± 7	hydrocarbon chain tilt from surface normal
d_{total} ($=d_{head} + d_{tail}$) (Å)	23.1 ± 0.5	total film thickness
A_0 ($=A_{DHDP} \cos \theta$) (Å)	40.7 ± 0.5	minimum cross-sectional area of lipid
$V_{phosphate}$ ($=A_{DHDP}d_{head} - N_{H_2O}V_{H_2O}$) (Å^3)	43.4 ± 3.0	volume of non-hydrated phosphate headgroup
V_{total} ($=V_{phosphate} + A_{DHDP}d_{tail}$) (Å^3)	851 ± 20	total volume of lipid molecule
constants		
A_{DHDP} (Å^2/molecule)	41	molecular area
$N_{e,tail}$	258	no. of electrons in hydrocarbon tail layer *per* lipid
$N_{e,phosphate}$	48	no. of electrons *per* phosphate headgroup
N_{e,H_2O}	10	no. of electrons *per* water molecule
V_{H_2O} (Å^3)	30	volume of water molecule

large plateau region between 4 and 7 mN/m for both DHDP/2,3-TMeAzPc and DHDP/TMePyP. This plateau is similar in shape to the liquid-expanded/liquid-condensed coexistence region observed for some glycerophospholipids and fatty acids.[36] Repeated compression and expansion of the DHDP/TMePyP film appeared to cause major structural changes in the monolayer, as evidenced by large hysteresis in consecutive isotherms.[37] Over many such compression/expansion cycles, the plateau region gradually disappeared, yielding a $\pi-A$ isotherm similar to those obtained for DHDP on the 3,4-CuTMeAzPc-containing subphase. This instability was also reflected in the difficulty in performing DHDP/TMePyP LB monolayer depositions (see section 2.1). These drastic changes in the $\pi-A$ behavior for DHDP/TMePyP do not reflect simple monolayer relaxation phenomena, such as surface pressure relaxation in fatty acid and phospholipid films when the compression/expansion process is halted. Large scale changes in film structure with compression/expansion cycling were subsequently verified by *in situ* X-ray reflectivity measurements.[37] In contrast, the isotherms for DHDP on H_2O and on both the phthalocyanine-containing subphases were nearly reversible.

3.2. X-ray Specular Reflectivity of Monolayers. The X-ray specular reflectivity of DHDP on H_2O and on the various pigment-containing subphases was measured at various points along their $\pi-A$ isotherms. Quantitative interpretation of specular reflectivities for lipid films at large molecular areas is often complicated by the presence of phase-segregated domain formation.[38,39] Detailed modeling of our data was therefore attempted primarily for molecular areas ≤ 50 Å^2/molecule (i.e., on data obtained from highly condensed phases, where $\pi > 20$ mN/m). However, differences in reflectivities at larger DHDP molecular areas on the various subphases also yield qualitative information about organizational similarities or differences between these films (see section 3.2.2.4). Some modeling was therefore performed on the expanded films (see also ref 18).

Electron density profiles were modeled using a sequence of "slabs" of constant electron density above the bulk subphase (see section 2.2). For DHDP and other simple fatty acid and phospholipid monolayers, the model is particularly simple and consists of two slabs: one slab contiguous to the bulk subphase (which contains the lipid headgroups and possibly waters of hydration), and a second slab adjacent to the air interface (which contains the hydrocarbon chain region). Modeling of the DHDP/pigment films is more complicated since one does not know *a priori* where to place the pigment slab, or even whether it exists as a discrete slab at all. We have considered placement of the pigment within the interfacial framework at three distinct locations: within the lipid molecular plane, at the hydrocarbon chain/air interface, and at the headgroup/bulk subphase interface. It is expected that if the pigment inserts into the lipid monolayer film, and does not constitute a layer unto itself, the extracted hydrocarbon electron densities for highly compressed films will have abnormal values compared to those in typical crystalline alkanes, DHDP on H_2O, or other lipid Langmuir monolayers. This model, however, is not supported by our extracted electron densities for the alkyl tail regions, which are characteristic of highly organized, densely packed hydrocarbon chains. In addition, linear dichroism measurements would indicate a near-normal orientation of the pigment plane (relative to the surface) for highly condensed phases, which is not observed (see section 3.3.1 and 3.3.3). We therefore infer that the pigment does not insert itself into the lipid film. Modeling an intact pigment slab on top of the hydrocarbon chain slab was also attempted. The extracted electron density profiles were unphysical, with abnormal electron densities and thicknesses. The most logical position for the pigment slab is underneath the lipid headgroup slab, nearest the bulk subphase (Figure 1), since this is the region in which Coulombic interactions between the headgroups and pigments are expected to occur. Recursive modeling using such an interfacial arrangement has yielded self-consistent results for all three pigment systems employed.

In the slab models adopted for DHDP on these various subphases, a three-dimensional "box" was constructed of cross-sectional area $A_{DHDP}(\pi)$, determined from the $\pi-A$ isotherm; each box was defined to contain one lipid molecule. For DHDP on H_2O, the phosphate headgroup and interfacial water molecules were partitioned into the subphase-adjacent slab of the box. The hydrocarbon chains were partitioned into the uppermost portion of this box. Although the reflectivity is directly related to the electron densities through eq 3, we have chosen not to use the densities as independent parameters. Rather, the electron densities are determined by other constraints imposed in the modeling (see below). The independent parameters emerging from the nonlinear least-squares analysis were (see Tables 1 and 2 for parameter definitions): (1) d_{tail} of the hydrocarbon region, from which ρ_{tail}, θ, and A_0 were calculated; (2) d_{head} and N_{H_2O} of the headgroup region, from which ρ_{head} and $V_{phosphate}$ were calculated; (3) the interfacial roughness σ. Included as constants in the fitting routine were A_{DHDP}, $N_{e,tail}$, $N_{e,phosphate}$, N_{e,H_2O}, and V_{H_2O} (see Table 1). For DHDP/pigment monolayers, a third slab was placed between the headgroup portion of the box and the subphase (see above). Into this portion of the molecular box, the pigment and additional interfacial water molecules were partitioned. The additional

TABLE 2: DHDP/Pigment Monolayer Structure at the Air/Water Interface

	DHDP/ 2,3-TMeAzPc	DHDP/ TMePyP
independent variables		
d_{tail} (Å)	17.0 ± 0.4	17.0 ± 0.3
d_{head} (Å)	2.4 ± 1.1	2.9 ± 1.1
$d_{pigment}$ (Å)	12.5 ± 0.2	8.0 ± 0.6
$N_{H_2O,head}$	0.6 ± 0.6	1.6 ± 1.6
$N_{H_2O,pigment}$	13.8 ± 0.6	9.8 ± 0.6
τ^a	0.231 ± 0.015	0.088 ± 0.015
σ (Å)	3.70 ± 0.05	3.14 ± 0.04
dependent variables		
ρ_{tail} (e/Å^3)	0.322 ± 0.004	0.322 ± 0.004
ρ_{head} (e/Å^3)	0.483 ± 0.020	0.467 ± 0.017
$\rho_{pigment}$ (e/Å^3)	0.435 ± 0.004	0.395 ± 0.007
θ (deg)	30.8 ± 1.8	30.9 ± 1.5
$d_{head+pigment}$ (Å)	14.9 ± 0.4	10.9 ± 1.8
d_{total} (Å)	32.0 ± 0.7	28.0 ± 2.1
$A_{pigment}{}^b$ (Å^2/molecule)	203 ± 15	534 ± 100
constants		
A_{DHDP} (Å^2/molecule)	47	47
$N_{e,pigment}{}^c$	518	574
$V_{pigment}{}^{d,e}$	762	941

[a] $\tau \equiv$ fraction of pigment per dialkyl phosphate (i.e., $1/\tau \equiv$ no. of DHDP's per pigment). [b] $A_{pigment} \equiv$ pigment molecular area $= A_{DHDP}/\tau$. [c] $N_{e,pigment}$ also includes electron contributions from four iodide counterions (4 × 54 e$^-$/iodide). [d] $V_{pigment}$ also includes volume contributions from four iodide counterions (4 × 44.6 Å^3/iodide). [e] Portion of $V_{pigment}$ contributed by chromophore calculated with Gaussian 92 for an AM1-optimized geometry.

independent parameters which emerged from this fit were $d_{pigment}$, $N_{H_2O,pigment}$, and τ of the pigment region, from which $A_{pigment}$ was calculated (see Table 2).

3.2.1. DHDP Monolayers on Pure H_2O. Figure 4a displays the reflectivity for DHDP on pure H_2O at 41 Å^2/molecule, near its limiting molecular area, plotted as the Fresnel-normalized reflectivity (R/R_F) versus the momentum transfer wave vector Q_z. The modulations found in R/R_F result from interference effects associated with variations in the electron density profile. The modulation amplitude is related to differences in the magnitude of the electron density, and the periodicity is inversely proportional to the distance between regions with different densities. As discussed above, the electron density can be modeled by the box model and the corresponding reflectivity can be calculated from eq 3. The solid curve shown in Figure 4a is the best fit to R/R_F for the box model and explains the essential features of the measured profiles. The corresponding density profile is displayed in the inset as a solid line. In the fitting, a single roughness parameter was used for all three interfaces, and the best fit results in $\sigma = 3.22$ Å. By eliminating the roughness (i.e., $\sigma = 0$), the nature of the box model is revealed and shown by the dashed line in the inset. Here, the bulk water subphase corresponds to $z < 0$ Å, the phosphate headgroup region corresponds to 0 Å $< z <$ 3.4 Å, and the alkyl tail region corresponds to 3.4 Å $< z <$ 23.1 Å. A full account of the parameters obtained from the fitting is listed in Table 1 along with their definitions. Confidence limits for each parameter, also listed in Table 1, were chosen based upon (1) a 50% increase in the minimum χ^2 values obtained by fixing the parameter of interest and allowing the others to vary[17] and (2) assuming a maximum error in the calculated molecular area A_{DHDP} of ±0.5 Å^2/molecule (~1% error) in the χ^2 analysis.[40]

The adjustable (i.e., independent) parameters are related to the electron density (in electrons/Å^3) of the tail and headgroup region, ρ_{tail} and ρ_{head}, respectively, through the simple algebraic relations

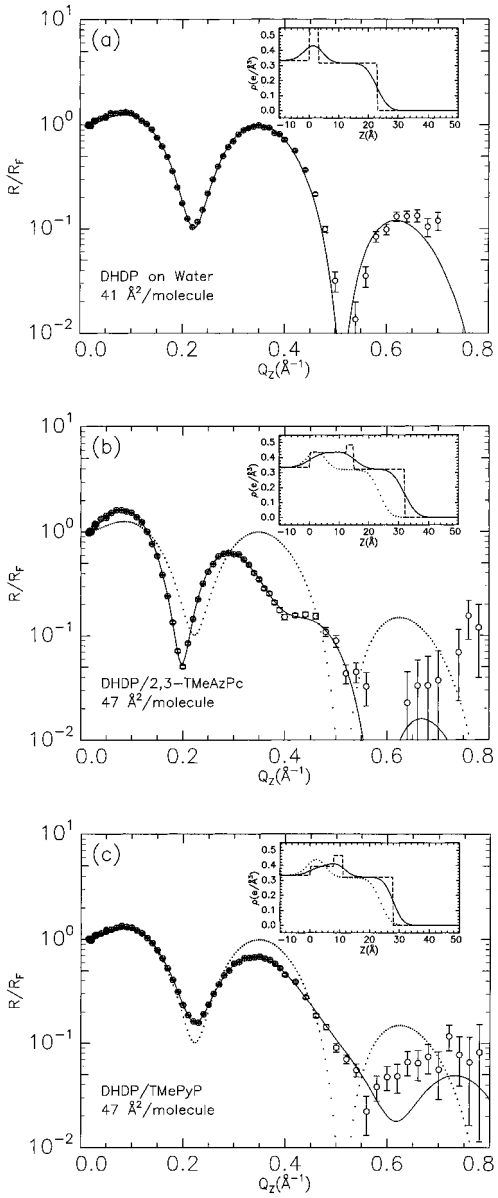

Figure 4. Normalized experimental (R/R_F) X-ray reflectivities, with corresponding best-fit electron density (ρ) models (shown in inset) for: (a) DHDP on H_2O (41 Å^2/molecule), (b) DHDP/2,3-TMeAzPc (47 Å^2/molecule), and (c) DHDP/TMePyP (47 Å^2/molecule). See text for a discussion of extracted molecular parameters and the resulting description of monolayer organization. Dotted curves in (b) and (c) are calculated reflectivities from DHDP on water.

$$\rho_{tail} = N_{e,tail}/A_{DHDP}d_{tail} \quad (6)$$

$$\rho_{head} = (N_{e,phosphate} + N_{H_2O}N_{e,H_2O})/A_{DHDP}d_{head} \quad (7)$$

where A_{DHDP} is the molecular area taken from the $\pi-A$ isotherm; all other parameters are defined in Table 1. Here the number of headgroup water molecules, N_{H_2O}, is related through eq 7 to the known values of $N_{e,phosphate}$, N_{e,H_2O}, and A_{DHDP}, and to the electron density profile parameters ρ_{head} and d_{head}. We implicitly assume water is entirely excluded from the hydrophobic hydrocarbon layer. This is reasonable under densely packed conditions; however, the nature of the hydrocarbon organization is not known *a priori*. One measure of its organization is the calculated value of ρ_{tail}. For highly organized, densely packed systems such as crystalline alkanes, $\rho_{tail}/\rho_{H_2O} \cong 1.00$, where $\rho_{H_2O} = 0.334$ electrons/Å^3. Simulated values of $\rho_{tail}/\rho_{H_2O} \gg 1.00$ are clearly unphysical. Ratios much lower than 1.00 suggest a fluid, porous hydrocarbon layer; tilt angle calculations based

on its thickness consequently may not be reliable. Therefore, interpretation of results in which substantial deviations occur from this relation should be strongly cautioned.

In addition, the volume of the phosphate moiety within the headgroup region can be calculated from the following relation

$$V_{\text{headgroup}} = A_{\text{DHDP}} d_{\text{head}} = (N_{\text{H}_2\text{O}} V_{\text{H}_2\text{O}}) + V_{\text{phosphate}} \quad (8)$$

where $V_{\text{H}_2\text{O}} = 30$ Å^3/molecule (extracted from the density of bulk water). The value of $V_{\text{phosphate}}$ thus extracted should be consistent with either known (e.g., based on X-ray crystallographic data or crystalline mass densities) or estimated (e.g., from CPK models) values. Therefore, $V_{\text{phosphate}}$ can be used as a measure of the reasonableness of the fit, and consequently of the picture of molecular organization within the system.

According to the model presented above, a molecular-level interpretation of the DHDP electron density profile at $A_{\text{DHDP}} =$ 41 Å^2/molecule (Figure 4a, inset) reveals the following:

(1) A hydrocarbon tail layer whose thickness (d_{tail}) is approximately 19.7 ± 0.4 Å and electron density (ρ_{tail}) is 0.319 ± 0.006 electrons/Å^3. The fact that $\rho_{\text{tail}}/\rho_{\text{H}_2\text{O}} \cong 0.955 \pm 0.018$ is consistent with a hydrocarbon tail region composed of densely packed alkyl chains, which resembles the results obtained from other closely packed fatty acid[16] and phospholipid[17] monolayer films. Assuming that the monolayer is closely packed with fully extended hydrocarbon tails, one can calculate the tilt angle θ of the molecule from the relation

$$d_{\text{tail}}/l_{\text{tail}} = \cos\theta \quad (9)$$

where l_{tail} is the full length of the extended alkyl chain. Since the methylene spacing projected onto the chain axis for crystalline saturated hydrocarbons is 1.265 ± 0.010 Å,[16] l_{tail} for DHDP can be calculated according to

$$l_{\text{tail}} = \{(N_{\text{CH}_2-\text{CH}_2} + {}^9/_8) \times 1.265 \text{ Å} + {}^1/_2 l_{\text{C-O}}\} \quad (10)$$

where $N_{\text{CH}_2-\text{CH}_2}$ is the number of methylene-methylene bonds ($N_{\text{CH}_2-\text{CH}_2} = 14$ for DHDP), ${}^9/_8$ is the portion of the length contributed by the terminal methyl substitutent,[16] and $l_{\text{C-O}}$ is the length of the carbon−oxygen bond ($l_{\text{C-O}} = 1.43 \pm 0.01$ Å). A similar relation has been utilized to estimate the chain length of arachidic acid;[16] however, that relation assumes that the electron density and bond length between the headgroup and nearest methylene unit is not significantly different than elsewhere along the chains and therefore contributes to the hydrocarbon layer thickness. Such assumptions lead to overestimation of the alkyl tail length for DHDP, and therefore to unreasonable calculated hydrocarbon chain tilt angles. (Their formulation[16] may be reasonable for a fatty acid such as arachidic acid, which exhibits a C−C bond between the carboxylic acid headgroup and the proximate CH_2 group; for DHDP, which has a C−O bond between the phosphate headgroup and the proximate CH_2, it probably overestimates the true hydrocarbon chain length.) Substitution of the appropriate values into eq 10 yields $l_{\text{tail}} = 19.84 \pm 0.16$ Å for DHDP. The calculated tilt angle θ (eq 9) measured at 41 Å^2/molecule is therefore 7° ± 7° relative to the surface normal (Table 1). (The rather large error associated with this parameter results from the insensitivity of the cosine function for angles near 0°.) This result correlates well with grazing incidence diffraction data for DHDP on H_2O, which indicates hexagonal subcell packing of the hydrocarbon tails (i.e., near-normal orientation of alkyl chains relative to interfacial plane).[41] The cross-sectional molecular area A_0 for DHDP perpendicular to the tilt axis is[16]

$$A_0/A_{\text{DHDP}} = \cos\theta \quad (11)$$

where $A_{\text{DHDP}} = 41$ Å^2/molecule. This yields $A_0 = 40.7 \pm 0.5$ Å^2/molecule, which compares favorably with that estimated from CPK models (41 ± 1 Å^2/molecule). This value is slightly larger than that expected for closely packed *crystalline* hydrocarbons (∼39.8 Å^2/molecule), however, and may be explained by the presence of a relatively high density of molecular scale defects (e.g., at domain boundaries). In addition, the value of A_0 reflects the true minimum molecular area since the cross-sectional area for the phosphate headgroup (∼24 Å^2 (ref 42)) is much smaller than that for two hydrocarbon chains (∼40 Å^2).

(2) A phosphate headgroup layer whose thickness d_{head} is 3.4 ± 0.8 Å and volume $V_{\text{phosphate}}$ is 43.4 ± 3.0 Å^3. (Recall from eq 8 that $V_{\text{phosphate}}$ is that of the "non-hydrated" headgroup.) Thus, the total thickness of the monolayer ($d_{\text{tail}} + d_{\text{head}}$) is 23.1 ± 0.5 Å, which is very near the CPK estimate (24.5 ± 0.5 Å). In addition, $V_{\text{phosphate}}$ agrees well with that calculated from X-ray crystallographic data of the structurally similar phospholipid dimyristoyl phosphatidic acid (DMPA) monosodium salt,[42] for which $V_{\text{phosphate}} = 36.5$ Å^3. (This value was obtained from the packing cross-sectional area of the phosphate ($A_{\text{phosphate}} = 24$ Å^2 (ref 42)), assuming a tetrahedral space-filling arrangement.) The close correspondence between these values underscores the quality of the fit and the reliability in the extracted parameters. The calculated value of ρ_{head} (=0.574 ± 0.250 electrons/Å^3) was much larger than that expected for a single phosphate alone, however, suggesting the presence of a headgroup hydration sphere with $N_{\text{H}_2\text{O}} = 3.2 \pm 1.4$. Evidence for a hydration sphere in the headgroup region of Langmuir monolayers is not unusual in X-ray specular reflectivity; the phosphatidylcholine headgroups in monolayers of DPPC contain nearly 4 associated water molecules each,[17] whereas a single H_2O is believed to be incorporated with each carboxylate headgroup of arachidic acid (AA) monolayers.[16] This is expected for a relatively small headgroup possessing a unit formal charge, since the presence of water as spacers permits more effective packing within the headgroup region and screens interheadgroup Coulombic repulsion. X-ray crystallographic studies of other lipid phosphates[42,43] show that the conformability between lipid tails and phosphate headgroups is enhanced by the ability of the phosphates to arrange themselves into strongly hydrogen-bonded strands, with spacer molecules residing between the strands. Thus, DHDP monolayers at the A/W interface appear to be an ideal system for studying the effects and structure of interfacial headgroup-bound water.

3.2.2. DHDP Monolayers on Pigment-Containing Aqueous Subphases. The addition of the pigments into the subphase has a profound effect on the X-ray reflectivity spectra of the DHDP monolayers and clearly indicates that the pigment must be incorporated into the surface region. The reflectivity of DHDP on the pigment-containing subphases was measured in both the compressed (<50 Å^2/molecule) and expanded (>50 Å^2/molecule) regions, at comparable molecular areas used for DHDP on H_2O. Due to the complex interactions and structural changes involved within the headgroup region upon introduction of the pigment, the electron density profiles were constructed as the sum of three slabs (i.e., pigment, phosphate headgroup, and hydrocarbon chains) in attempts to characterize the interfacial film structure. Interfacial H_2O was quantified within both the pigment and phosphate headgroup slabs; the hydrocarbon tail region was defined as before.

In order to evaluate pigment organization at the interface, constraints were placed on the electron density and volume contributions made by such molecules. The electron density within the box that contains the pigment was defined according to

$$\rho_{\text{pigment}} = (\tau N_{\text{e,pigment}} + N_{\text{H}_2\text{O,pigment}} N_{\text{e,H}_2\text{O}})/(A_{\text{DHDP}} d_{\text{pigment}}) \quad (12)$$

where τ is the fraction of pigment per lipid, and the other terms are defined in Tables 1 and 2. An additional constraint is applied through the volume of the box, so that

$$V_{\text{pigment box}} = A_{\text{DHDP}} d_{\text{pigment}} = \tau V_{\text{pigment}} + N_{\text{H}_2\text{O,pigment}} V_{\text{H}_2\text{O}} \quad (13)$$

where the volume of the pigment V_{pigment} was calculated with the set of quantum codes Gaussian 92 for the AM1-optimized geometry.[44] The independent parameters emerging from the nonlinear least-squares analysis were (see Table 2) (1) d_{tail} of the hydrocarbon region, from which ρ_{tail} and θ were calculated; (2) d_{head} and $N_{\text{H}_2\text{O,head}}$, from which ρ_{head} was calculated; (3) d_{pigment}, $N_{\text{H}_2\text{O,pigment}}$, and τ, from which ρ_{pigment} and A_{pigment} were calculated under the electron density and volume constraints outlined in eqs 12 and 13; (4) the interfacial roughness σ. Confidence limits for each parameter in these DHDP/pigment monolayer systems, also listed in Table 2, were chosen based upon the same criteria as for DHDP on pure H_2O.

3.2.2.1. DHDP/2,3-TMeAzPc MLs. Figure 4b displays the normalized reflectivity for DHDP on 1 μM 2,3-TMeAzPc aqueous subphase at 47 Å^2/molecule (near the limiting molecular area of DHDP). The simulated reflectivity (solid curve) is computed from the density profile (inset) obtained via least-squares analysis of the experimental reflectivity. Also included in the figure for comparison is the calculated reflectivity for DHDP on pure H_2O at 41 Å^2/molecule (dotted curve; see also Figure 4a) and its corresponding density profile (dotted curve in inset). Substantial differences clearly arise from the presence of 2,3-TMeAzPc in the subphase. These differences clearly argue in favor of an interfacial pigment film, which is expected to be localized at the A/W interface through attractive Coulombic forces with the lipid headgroup film.

A molecular interpretation of the electron density profile (Figure 4b, inset, and Table 2) reveals:

(1) A hydrocarbon chain tilt angle $\theta = 30.8° \pm 1.8°$. This result appears to be significantly greater than that for DHDP on pure H_2O at comparable high surface pressures (Table 1). The larger tilt angle implies that DHDP is somewhat expanded on the 2,3-TMeAzPc-containing subphase relative to pure water. This is also evidenced by the larger average molecular areas observed in the DHDP/2,3-TMeAzPc $\pi-A$ isotherms; the pigment therefore influences lipid organization. The electron density ratio $\rho_{\text{tail}}/\rho_{\text{H}_2\text{O}}$ is 0.964 ± 0.012, which suggests that the hydrocarbon tail region is well-ordered and densely packed, similar to that for DHDP on pure water.

(2) A combined (2,3-TMeAzPc + phosphate headgroup) layer thickness ($d_{\text{pigment+head}}$) of 14.9 ± 0.4 Å. Although this combined thickness seems rather large in light of the expected space-filling contributions from both a phosphate layer (~4−5 Å) and a coplanar phthalocyanine layer (~3−4 Å), there are several explanations for such an observation which deserve examination. An out-of-plane pigment arrangement (which would also produce large values of $d_{\text{pigment+head}}$) can be dismissed on the basis of the calculated value of A_{pigment} from X-ray reflectivity (Table 2) and optical measurements (see section 3.3.1), and from linear dichroism studies (section 3.3.1). In addition, one must consider the potential contributions of interfacial H_2O (~13.8 molecules) and the iodide counterions. While modeling describes the excess electron density (relative to that for the pigment and phosphate combined) within the $d_{\text{pigment+head}}$ region, neither the electron density distribution normal to the interface nor the chemical identity of the species from which this excess originates is known *a priori*. In fact, it is not unreasonable to assume that an interfacial layer of iodide (the phthalocyanine counterion) exists underneath the 2,3-TMeAzPc layer. The inclusion of an iodide layer (ionic radius (I^-) = 220 pm) into the CPK-estimated thickness $d_{\text{pigment+head}}$ (~7−9 Å) would result in an overall headgroup interfacial width of 11−13 Å, which is near that which emerges from the fit ($d_{\text{pigment+head}}$ = 14.9 Å). (In addition to the iodide layer, incorporation of interfacial H_2O into this picture would likely result in interfacial widths near that extracted from the fit.) In addition, *in situ* grazing incidence X-ray diffraction of DHDP/2,3-TMeAzPc at these molecular areas[41] has evidenced highly crystalline two-dimensional films with lattice spacings corresponding to phthalocyanine dimensions. These diffraction results indicate that, if present, the iodide does not reside within the plane containing the phthalocyanine pigments since such an organization would result in considerably larger lattice dimensions. Because of their highly rigid, planar, symmetric molecular structure, phthalocyanines form highly crystalline thin films[45] and therefore it is surmised that the steric requirements for achieving such order within the plane containing the pigments results in exclusion of any entrained iodide counterions. While the presence of iodide within the film cannot be confirmed or denied from these reflectivity results alone, it is anticipated that they form a layer underneath the phthalocyanine plane through attractive Coulombic association (Figure 5a). Since iodide is a heavy element, its X-ray fluorescence yield is

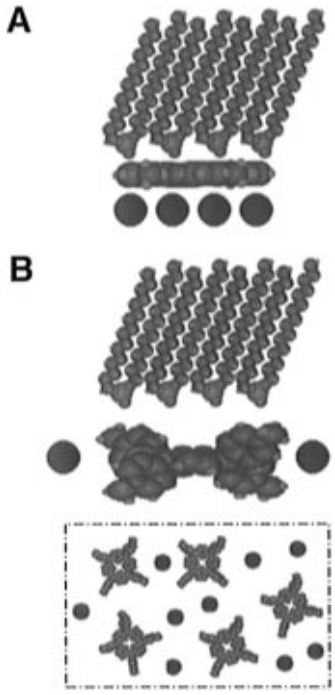

Figure 5. Depiction of interfacial organization of DHDP/pigment monolayers (along the interfacial plane), showing predicted location of iodide counterions, for (a) DHDP/2,3-TMeAzPc and (b) DHDP/TMePyP. Interfacial water is excluded for clarity. Inset in (b) illustrates organization of TMePyP and iodide counterions within pigment plane (i.e., observed along surface normal). This depiction presents one possible interpretation of the X-ray reflectivity-derived electron density profile; models involving a slight tilt of the pigments relative to the interfacial plane cannot be excluded.

high, and therefore its position along the interface normal may be ascertained through X-ray standing wave (XSW) studies.[46,47] Such investigations should be able to determine if such a counterion organization exists within these DHDP/2,3-TMeAzPc monolayers.

(3) A total DHDP/2,3-TMeAzPc layer thickness (d_{total}) of 32.0 ± 0.7 Å. This accounts for the combined changes in monolayer thickness due to pigment incorporation and increases in hydrocarbon tilt angle.

(4) A 2,3-TMeAzPc/DHDP ratio (τ) of 0.231 ± 0.015, which corresponds to approximately 4.33 ± 0.30 DHDP's per 2,3-TMeAzPc.

(5) A pigment molecular area ($A_{pigment}$) of approximately 203 Å^2/molecule. This is in excellent agreement with the CPK value expected for interfacially coplanar 2,3-TMeAzPc chromophores ($A_{pigment} \cong (14.2\ Å)^2 = 202$ Å^2/molecule), and with the molecular areas determined from optical measurements of LB monolayers (∼255 Å^2/molecule, see section 3.3.1). This result indicates a close-packed, coplanar arrangement of pigments at the A/W interface.

(6) An interfacial roughness (σ) of 3.70 ± 0.05 Å. The extracted roughnesses for both phthalocyanine-containing monolayers (Table 2) are somewhat larger than that for DHDP alone or DHDP/TMePyP.

3.2.2.2. DHDP/3,4-CuTMeAzPc MLs. The normalized reflectivity for DHDP on a saturated 3,4-CuTMeAzPc aqueous subphase has been measured at various points along its $\pi-A$ isotherm and quantitatively analyzed at 45 Å^2/molecule.[18] Although the reflectivities for DHDP on the two phthalocyanine-containing subphases (2,3-TMeAzPc and 3,4-CuTMeAzPc) differ considerably, quantitative interpretation of DHDP/3,4-CuTMeAzPc interfacial organization in a manner analogous to the 2,3-TMeAzPc-containing films has not been straightforward. The difficulty in obtaining high-quality least-squares fits to the reflectivity data may be a consequence of the nature of the adsorbed pigment species. Optical spectra of 3,4-CuTMeAzPc in aqueous solution indicate that the pigment exists in an aggregated state (see section 3.3.2), and spectra of LB monolayers on quartz suggest that these aggregates exist within the film also. This is in sharp contrast to what is known about the nature of the 2,3-TMeAzPc and TMePyP aqueous solution species (see sections 2.3, 3.3.1, and 3.3.3); the reflectivities of these two DHDP/pigment systems can be easily simulated employing a simple three-box model wherein the pigment box is defined to include unaggregated (i.e., monomeric) pigment species. The nature of the aggregate state for 3,4-CuTMeAzPc is unknown and therefore may explain the difficulty in obtaining reasonable least-squares fits to the reflectivity data.

A preliminary optimized density profile has yielded an interfacial structure which is quite different than that of DHDP/2,3-TMeAzPc. Qualitatively, the most notable difference has been a decrease in $d_{pigment+head}$ in the DHDP/3,4-CuTMeAzPc system ($d_{pigment+head} = 6.8$ Å), which may stem from a much smaller number of interfacial water molecules ($N_{H_2O,total} = 4.3$). The calculated pigment molecular area ($A_{pigment}$) for DHDP/3,4-CuTMeAzPc is 450 Å^2/molecule, which is more than twice that for the DHDP/2,3-TMeAzPc system. For comparison, the expected CPK cross-sectional area for a single 3,4-CuTMeAzPc is approximately 210 Å^2/molecule. This interesting result correlates with solution and LB film optical measurements (section 3.3.2), which suggest that spontaneous aggregation occurs with this pigment. In addition, since $\rho_{tail}/\rho_{H_2O} \cong 0.934$, the hydrocarbon tails may not be quite as densely packed as those in the previous two systems, and therefore extrapolation of alkyl tilt angles may not be reliable.

3.2.2.3. DHDP/TMePyP MLs. Figure 4c displays the normalized reflectivity for DHDP on a 1 μM TMePyP aqueous subphase at 47 Å^2/molecule, near its limiting molecular area. Included in the figure for comparison is the calculated reflectivity for DHDP on pure H_2O at 41 Å^2/molecule (dotted curve, see also Figure 4a) and its corresponding density profile (dotted curve in inset). The extracted parameters (Table 2) correspond to the following:

(1) A hydrocarbon tilt angle $\theta = 30.9° \pm 1.5°$, very similar to that for DHDP/2,3-TMeAzPc.

(2) A $d_{pigment+head}$ of 10.9 ± 1.8 Å, which is about one-third smaller than that for DHDP/2,3-TMeAzPc. As with DHDP/2,3-TMeAzPc, the moderately large $d_{pigment+head}$ could potentially be attributed to a nonparallel TMePyP orientation (relative to the interfacial plane) and/or greater thickness of tetraarylporphyrins in general relative to phthalocyanines (due to the known buckling of the porphine skeleton and the near-orthogonal orientation of the aryl groups with respect to the porphine plane[48]). Linear dichroic measurements, however, favor a coplanar pigment arrangement. Since the total number of interfacially bound H_2O's is significantly less than that in the DHDP/2,3-TMeAzPc film, the smaller value of $d_{pigment+head}$ may reflect this difference. A more likely explanation for this decrease, however, may reside in the location of interfacially bound iodide counterions. The difference in the extracted value of $d_{pigment+head}$ between the 2,3-TMeAzPc- and TMePyP-containing films is 4.0 ± 2.2 Å, which is approximately the diameter of an iodide species. This implies that the iodide species do not form a counterion layer underneath the plane containing the pigments. If the iodides were allowed to exist in the plane *with* the TMePyP pigments, the average pigment molecular area $A_{pigment}$ would likely increase (Figure 5b). One can estimate that the value of $A_{pigment}$ might vary from approximately $(17\ Å)^2 \cong 290$ Å^2/molecule (space-filling estimate with no iodide in pigment plane) to nearly $(23\ Å)^2 \cong 530$ Å^2/molecule (assuming iodide association at the corners of the TMePyP "square", nearest the pyridyl methyl groups). The reflectivity value of $A_{pigment}$ (534 ± 100 Å^2/molecule) is consistent with this qualitative picture of interfacial organization, and with optical density-extracted molecular areas (∼615 ± 70 Å^2/molecule, see section 3.3.3), both of which are considerably larger than space-filling estimates ($A_{pigment}$(CPK) ≅ 290 Å^2/molecule). Incorporation of iodide within the plane containing the TMePyP pigments, coupled with the less rigid nature of the porphyrin relative to the phthalocyanine, may also likely explain our inability to obtain *in situ* grazing incidence X-ray diffraction data from these DHDP/TMePyP monolayers.[41] As with the 2,3-TMeAzPc-containing films, the location of the iodide counterions along the surface normal may be ascertained through XSW measurements.[46,47]

(3) A pigment/dialkyl phosphate ratio τ of 0.088 ± 0.015, which corresponds to approximately 11.4 ± 2.3 DHDP's per TMePyP.

3.2.2.4. DHDP/Pigment MLs at Molecular Areas > 50 Å^2/molecule. Experimental and simulated reflectivities for DHDP on H_2O, 1 μM 2,3-TMeAzPc, and 1 μM TMePyP are shown for several lipid molecular areas (A_{DHDP}) in Figure 6a−c, respectively. (Reflectivities from each clean subphase surface are also shown for comparison.) Even for molecular areas as large as 90 Å^2/molecule on pure H_2O (Figure 6a), a film-specific signature is discernible. For DHDP on H_2O, attempts to fit the experimental data at these larger molecular areas using the two-slab model employed for the densely packed film (Table 1) were largely unsuccessful. *In situ* grazing incidence X-ray diffraction measurements at similar molecular areas have revealed diffrac-

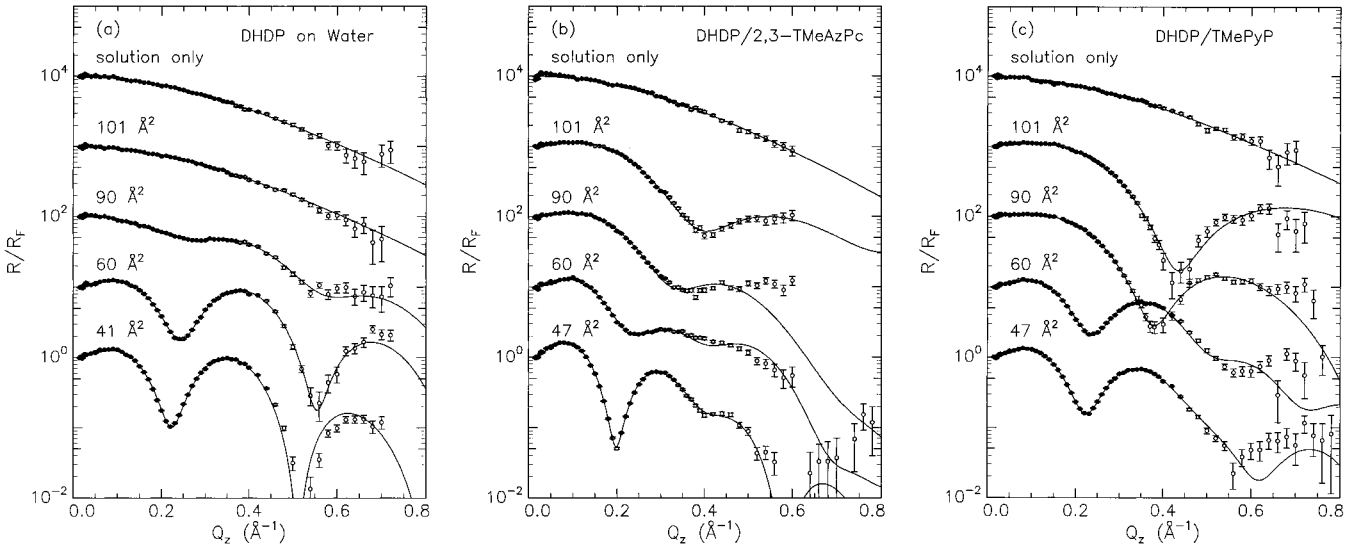

Figure 6. Normalized experimental (R/R_F) and calculated X-ray reflectivities for DHDP on (a) H_2O, (b) 1 μM 2,3-TMeAzPc, and (c) 1 μM TMePyP subphases as a function of lipid molecular area. Ordinate axes are each offset by an order of magnitude for clarity. See text for a discussion of extracted molecular parameters and the resulting description of monolayer organization as the DHDP film is compressed.

tion maxima, suggesting the presence of two-dimensional phase segregation.[41] To account for this lateral nonuniformity, the reflectivities were modeled as linear combinations of those in the densely packed phase (R_{film}) and the bare subphase surface (R_F):

$$R(Q_z) = \alpha R_{film} + (1 - \alpha)R_F \qquad (14)$$

where α is the fractional surface coverage occupied by the monolayer. The overall reflectivity at 90 Å^2/molecule was approximated quite well assuming 60% surface coverage by the highly compressed phase; at 60 Å^2/molecule, an 86% coverage resulted in a high quality fit (Figure 6a). This analysis supports the notion that domain formation occurs, similar to that commonly observed in monomolecular films at the A/W interface.[38]

In contrast, DHDP films on both pigment-containing subphases exhibit very prominent reflection minima at all points within the $\pi-A$ isotherm, even at very large lipid molecular areas (Figure 6b,c). Their appearance signals the presence of intact, uniformly distributed films at the A/W interface. In comparison with DHDP on H_2O, these pronounced minima occurring at large molecular areas suggest that the signal originates from an intact 2,3-TMeAzPc layer at the A/W interface. This observation is supported by LB monolayer transfer experiments (section 3.3.4), in which the pigment surface density is found to be quite insensitive to the degree of compression of the DHDP monolayer within the $\pi-A$ isotherm.

Despite the highly expanded nature of the DHDP layer at these molecular areas, some preliminary modeling was attempted using a two-box model in which both the phosphate headgroup and alkyl tails were confined to the uppermost slab. Recursive least-squares analysis of these data (Figure 6b,c) has indicated that the pigment/lipid ratio (τ) changes as the film is compressed (Table 3). This demonstrates that, although the lipid and pigments are strongly associated, their mutual stoichiometry depends on the degree of compression. The extracted pigment molecular areas are tabulated versus lipid molecular area (A_{DHDP}) in Table 3. For DHDP/TMePyP films, $A_{pigment}$ remains fairly constant (within the error displayed in Table 2) as the lipid film is compressed (within the range of lipid molecular areas examined). This correlates well with optical absorption spectra of transferred DHDP/TMePyP monolayers, where little or no change in pigment surface densities is observed over a 2−3 magnitude variation in lipid molecular area (see section 3.3.4). For the DHDP/2,3-TMeAzPc films, however, some variability was observed in reflectivity-extracted values of $A_{pigment}$ across the same range of DHDP molecular areas. Some of this variability in τ, and therefore in $A_{pigment}$, is certainly a reflection of imperfect nonlinear least-squares fits. Since optical density measurements (section 3.3.1) have also indicated virtually no change in the 2,3-TMeAzPc surface density as the DHDP film is compressed, further analysis and modification of the DHDP/2,3-TMeAzPc film model are required. These preliminary analyses, however, do demonstrate the existence of an intact, uniform pigment layer at all DHDP molecular areas measured.

TABLE 3: DHDP/Pigment Monolayer Organization as a Function of Lipid Molecular Area

	A_{DHDP} (Å^2/molecule)	τ	$A_{pigment}$ (Å^2/molecule)
2,3-TMeAzPc	47	0.231	203
	60	0.144	417
	90	0.159	566
	101	0.214	472
TMePyP	47	0.088	534
	60	0.148	405
	90	0.168	536
	101	0.224	451

3.3. Optical Spectroscopy of Transferred Monolayers. Electronic absorption spectra were acquired for monomolecular DHDP/pigment films transferred onto solid support via LB methodology.[19,36] These films were transferred at a variety of molecular areas (or surface pressures) in order to determine whether or not the lipid organization influences the pigment density. Pigment molecular areas (in Å^2/molecule) or surface densities (in mol/cm^2) for each film were extracted from the visible optical spectra, and mean chromophore orientations were determined via linear dichroism measurements (see section 2.3). For both DHDP/2,3-TMeAzPc and DHDP/TMePyP, good agreement in the pigment molecular areas has been obtained from both X-ray reflectivity and optical density measurements. This result, combined with the appearance of the visible spectra of the monolayer films relative to that in solution, supports the assumption that the pigment optical absorption coefficients change very little (other than by a small factor that accounts for their anisotropic arrangement within the film, see section 2.3) both upon incorporation within the film and upon deposition

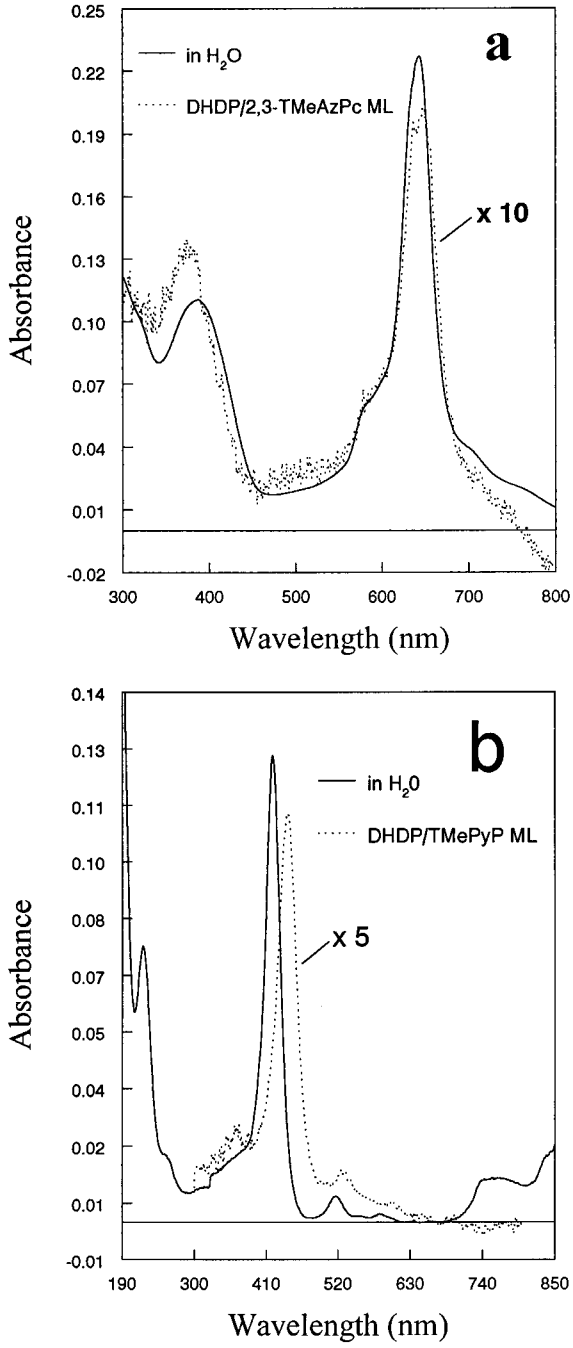

Figure 7. Electronic absorption spectra of chromophores both in solution and in transferred DHDP/pigment LB monolayers ($\pi_{transfer}$ = 20.0 mN/m): (a) 2,3-TMeAzPc and (b) TMePyP.

onto the substrate, relative to the solution monomeric value. Linear dichroism studies have indicated similar mean molecular orientations for both films. The comparability between these results for both systems has demonstrated the existence of a single, monomolecular pigment layer.

3.3.1. DHDP/2,3-TMeAzPc LB MLs. Figure 7a displays absorption spectra of 2,3-TMeAzPc in aqueous solution and incorporated within a DHDP/2,3-TMeAzPc ML transferred onto a quartz slide ($\pi_{transfer}$ = 20.0 mN/m). In aqueous solution, the Q-band spectrum (550−700 nm) of 2,3-TMeAzPc is characteristic of monomeric phthalocyanine and indicates an absence of aggregation;[11] this has also been confirmed by electron spin resonance for the corresponding Cu(II) complex.[49] Upon transfer of a DHDP/2,3-TMeAzPc monolayer to a quartz substrate, there is virtually no shift or broadening in the Q-band spectrum relative to that in solution. Since excitonic coupling within cofacial arrays of phthalocyanines and similar chromophores produces significant changes in these properties,[50] the virtual absence of peak shifting and broadening argues strongly against the presence of aggregates within the film and in favor of monomeric pigments. (Small spectral shifts are attributable to solvatochromic effects, since the pigment environment within the monomolecular film differs slightly from that in solution.[51]) These results reported here contrast with the bulk of the phthalocyanine Langmuir and LB film literature. For example, studies with metalated *N*,*N*′,*N*″,*N*‴-tetraoctadecyltetra-3,4-pyridinoporphyrazine (similar to 3,4-CuTMeAzPc, except that quaternization was performed with *n*-octadecylbromide rather than methyl iodide in order to introduce amphiphilic character to the Pc[52,53]) reported substantial shifting and broadening in the optical bands for ∼180-layer LB film samples. (Indeed, these spectra are quite similar to the aqueous solution spectra of 3,4-CuTMeAzPc; cf. next section.) The only study known to us utilizing an interfacial complexation approach based on water-soluble, ionic phthalocyanines is that of Palacin and Barraud.[14] Although these authors presented no optical spectra, their phthalocyanine was the cobalt-metalated version of 3,4-CuTMeAzPc, which from our studies appears to aggregate in aqueous solution (see section 3.3.2).

The molecular surface density of 2,3-TMeAzPc within the LB monolayer, extracted from the optical density of the $S_0 \rightarrow S_1$ transition at 645 nm (Figure 7a), is $(6.5 \pm 0.4) \times 10^{-11}$ mol/cm^2, which corresponds to a pigment molecular area of 255 ± 15 Å^2/molecule. This is similar to the CPK estimate of ∼202 Å^2/molecule and the reflectivity result of 203 Å^2/molecule and evidences a coplanar arrangement of pigments at the interface. Average molecular tilt angles (θ) were calculated independently by optical linear dichroism measurements of the same samples. Since group theoretical considerations demonstrate that the transition dipole associated with the $S_0 \rightarrow S_1$ transition is polarized in the plane of the azaphthalocyanine pigment, determination of the pigment orientation relative to the substrate surface is straightforward.[29−34] Such calculations yielded an average 2,3-TMeAzPc tilt angle of $\theta = 65° \pm 5°$ from the surface normal, which corresponds to a "projected area" of the pigment on the substrate surface of approximately 183 Å^2/molecule (assuming the CPK molecular dimensions of 14 Å × 14 Å). These results collectively suggest that an unaggregated pigment layer is Coulombically associated with the lipid film. Beyond the problems associated with other phthalocyanine-containing LB films, our system is interesting in the light of difficulties typically encountered in the vapor deposition of films composed of large planar chromophores.[54] With vapor deposition methods, such as organic molecular beam epitaxy (OMBE),[54] control over the film structure and morphology is maintained through low deposition rates (<1 monolayer/h) and elevated substrate temperatures. This may not achieve layer-by-layer (Frank−Van der Merwe[55]) film growth in systems where $\pi-\pi$ cofacial interactions are substantial. In the OMBE growth of chloroindium phthalocyanine monolayers on metal dichalcogenide surfaces[49,56] at coverages near one equivalent monolayer, significant shifts (>50 nm) and broadening are observed in the phthalocyanine optical spectrum relative to its solution spectrum. Thus, it may be impossible to eliminate completely three-dimensional nucleation (Stranski−Krastanov growth[55]) with vapor deposition methods. In contrast, the attractive Coulombic forces (which serve to isolate the pigment at the A/W interface) and the intermolecular Coulombic repulsions (within the pigment plane) combine to produce a truly monomeric chromophore assembly in our DHDP/2,3-TMeAzPc films. This fact, in conjunction with the intense $S_0 \rightarrow S_1$ transition in monomeric

phthalocyanines, endows our system with potential as an artificial photosynthetic antenna.

3.3.2. DHDP/3,4-CuTMeAzPc LB MLs. Optical spectra for 3,4-CuTMeAzPc in solution and in a DHDP/pigment film transferred to quartz ($\pi_{transfer} = 20.0$ mN/m) have been obtained but are not shown. Whereas the solution spectrum in 1-chloronaphthalene is characteristic of monomeric azaphthalocyanines, the spectrum obtained in aqueous solution is quite different and suggests that aggregation occurs. (The very low solubility of this pigment in aqueous solution accounts for a substantial decrease in intensity in this region. Indeed, it is interesting that the aqueous solution spectrum we have observed is similar in appearance to that displayed for multilayer LB films of tetracationic tetraazaphthalocyanines quaternized with long alkyl chains.[52,53]) The extreme broadening observed in the electronic spectrum upon aggregation in aqueous solution may contribute to our inability to obtain a visible absorption spectrum from an LB monolayer. Although the nature of the 3,4-CuTMeAzPc aggregation mechanism and complex is unknown at present, the effect of reagent purity cannot be ruled out as its possible source (section 2.1). The interfacial pigment density of 3,4-CuTMeAzPc is not believed to be substantially different than that of 2,3-TMeAzPc, since our X-ray reflectivity data and isotherms indicate its presence at the DHDP/aqueous solution interface. If the interfacial density of 3,4-CuTMeAzPc were much different, the $\pi-A$ isotherms would likely not converge to the same limiting molecular area as observed with the other two pigment systems.

3.3.3. DHDP/TMePyP LB Monolayers. Optical spectra for TMePyP in aqueous solution and transferred as a monomolecular DHDP/TMePyP film to quartz ($\pi_{transfer} = 20.0$ mN/m) are shown in Figure 7b. The aqueous solution spectra evidence a large Soret (or B) band at 421 nm, and much less intense Q-bands between 475 and 650 nm; these spectra are already well established.[28,57] Previous absorbance[57] and fluorescence[58] measurements over an extensive concentration and pH range have indicated that TMePyP exists predominantly as a monomer in aqueous solution below 10^{-3} M. Upon transfer of a DHDP/TMePyP monolayer to quartz, a small red shift ($\sim$15$-$20 nm) and slight increase in broadening ($\sim$7%) is observed relative to that in solution. Both are slightly larger than that observed for DHDP/2,3-TMeAzPc MLs. These effects typically appear to be more common and more pronounced in spread Langmuir monolayer films of long-chain hydrocarbon-modified porphyrins (compared to those formed via the Coulombic route described here),[59$-$62] although there are exceptions.[63] To date, only three other studies using the interfacial complexation method for porphyrin films have been reported.[13,61,64] Changes in the optical spectra in one study[61] were complicated by Cd^{2+} complexation of the free-base porphyrin directly at the A/W interface, whereas the others[13,64] were the systems which motivated our investigations.

The pigment surface densities within the DHDP/TMePyP ML were calculated from the optical density of the Soret band and are $(2.7 \pm 0.3) \times 10^{-11}$ mol/cm^2. This corresponds to a molecular area of 615 ± 70 Å^2/molecule, which indicates a mean pigment separation of $\sim$25 Å. These molecular areas agree well with those extracted from X-ray reflectivity results near the limiting DHDP molecular area ($A_{pigment} \cong 534 \pm 100$ Å^2/molecule) and indicate an expanded pigment layer. This increase in $A_{pigment}$ relative to the space-filling estimate ($\sim$290 Å^2/molecule) was explained from the reflectivity measurements as resulting from incorporation of the iodide counterions into the plane containing the TMePyP pigments (section 3.2.2.3 and Figure 5b). In addition, linear dichroism measurements of the Soret region on transferred LB monolayers evidence an average molecular tilt angle of $\theta = 70° \pm 5°$, similar to that for 2,3-TMeAzPc, and consistent with the coplanar pigment arrangement deduced from the TMePyP reflectivity results. (From group theoretical considerations, the electronic transition moments associated with the porphyrin Soret and Q-bands are polarized in the plane of the porphine skeleton.) Judging from these results, the portrayal of monolayer structure previously advanced[13] is rather idealized judging from these X-ray specular reflectivity and optical spectroscopic results.

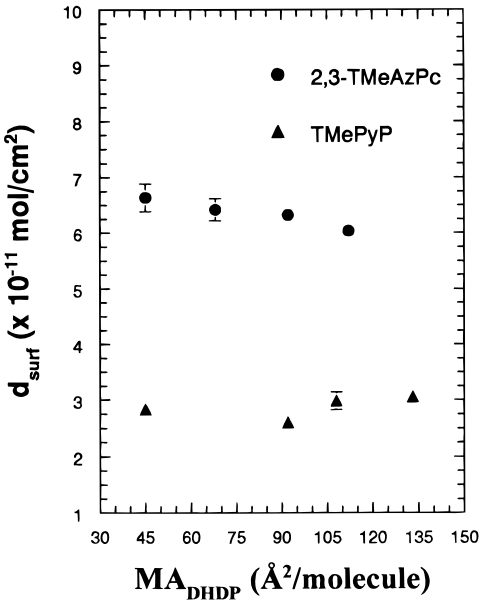

Figure 8. Plot of pigment surface density (d_{surf}) as a function of the molecular area of the spread lipid DHDP (A_{DHDP}). Pigment surface densities were calculated from the measured optical densities of the absorption bands at 645 nm (2,3-TMeAzPc) and at 440 nm (TMePyP). (See Figure 6, a and c.)

3.3.4. DHDP/Pigment Monolayers at Molecular Areas > 50 Å^2/molecule. Optical spectra have been obtained for both the DHDP/2,3-TMeAzPc and DHDP/TMePyP systems at molecular areas > 50 Å^2/molecule. A plot of each pigment's molecular surface density (calculated from the observed optical densities) versus DHDP molecular area is shown in Figure 8. There appears to be little or no (<10%) overall change in the interfacial density of either pigment as the lipid film is compressed. This is striking since, during the compression, the molecular area of DHDP changes by 200$-$300%. Although the exact mechanism is unclear, it is apparent that at these lipid molecular areas, the pigment interfacial density does not vary substantially and because of interpigment Coulombic repulsion resists the compression force. The notion that the pigments may not be absolutely isolated at the A/W interface as the lipids are, but can potentially redissolve back into the subphase, may provide the crucially needed escape route by which they avoid being overcompressed and becoming too tightly packed. In addition, since the pigments cannot stably exist at the A/W interface without complexing with the lipid, the nearly constant pigment densities imply that the lipid is somewhat homogeneously distributed across the film even at large DHDP molecular areas; in other words, no large bare areas appear to exist on the subphase surface. Further investigations of this interesting phenomenon are currently in progress.

4. Summary

In conclusion, monomolecular assemblies of cationic tetraazaphthalocyanines unaffected by aggregation have been

created for the first time. The natural tendency for these pigments to self-aggregate (due to strong $\pi-\pi$ interactions) in the complexed state at the A/W interface appears to be overridden both by the strong repulsive Coulomb interactions between neighboring positively charged macrocycles and by the attractive Coulomb interactions with the negatively charged phosphate headgroups of the spread DHDP film. The phthalocyanine molecular areas obtained via specular X-ray reflectivity, and optical density measurements on transferred LB monolayers, are in very good agreement and indicate a monomolecular, close-packed, coplanar 2,3-TMeAzPc film residing underneath the lipid Langmuir monolayer. Film thicknesses extracted from X-ray reflectivity also suggest the presence of an iodide counterion layer underneath the 2,3-TMeAzPc pigment layer. For comparison, similar films containing the cationic porphyrin TMePyP were also examined. The close correspondence between TMePyP molecular areas obtained from X-ray reflectivity and optical density measurements indicates that these pigments are also primarily unaggregated. These larger TMePyP pigment areas (in contrast to that expected from space-filling estimates) suggest a more expanded pigment layer, wherein iodide counterions might reside. The location of iodide counterions within the TMePyP-containing layer is also supported by decreased film thicknesses obtained via X-ray reflectivity. This portrait of interfacial organization is in sharp contrast to that obtained for the 2,3-TMeAzPc-containing films. In addition to the extensive X-ray reflectivity and optical measurements on these pigment-complexed monolayers, particular attention has also been directed toward a molecular-level description of the DHDP monolayer itself and its relationship to that obtained from similar lipid monolayers such as arachidic acid and dipalmitoylphosphatidylcholine. Grazing incidence X-ray diffraction results from these films will be reported in a future publication.[41]

Acknowledgment. The Ames Laboratory is operated for the U.S. Department of Energy by Iowa State University under Contract No. W-7405-Eng-82. This work was supported by the Division of Chemical Sciences, Office of Basic Energy Sciences. We thank Professor A. E. DePristo for many useful discussions during the early phases of this work, and Professor M. S. Gordon, Dr. M. W. Schmidt, and V. A. Glezakou for assisting with the Gaussian 92 calculations. We would also like to thank the late Dr. Robert A. Uphaus for his inspiration in the initial stages of this project and Dr. Brian Cooper for his assistance with modifications of the monolayer trough. The work at Brookhaven National Laboratory was also supported by the Department of Energy under Contract No. DE-AC02-76CH00016.

References and Notes

(1) Moore, J. S.; Zhang, J. *Angew. Chem., Int. Ed. Engl.* **1992**, 922.
(2) Wagner, R. M.; Ruffing, J.; Breakwell, B. V.; Lindsey, J. S. *Tetrahedron Lett.* **1991**, *32*, 1703.
(3) Bignozzi, C. A.; Argazzi, R.; Garcia, C. G.; Scandola, F.; Schoonover, J. R.; Meyer, T. J. *J. Am. Chem. Soc.* **1992**, *114*, 8727.
(4) Gust, D.; Moore, T. A.; Moore, A. L.; Lutrell, D. K.; DeGraziano, J. M.; Boldt, N. J.; Van der Auweraer, M.; DeSchryver, F. C. *Langmuir* **1991**, *7*, 1483.
(5) *Anoxygenic Photosynthetic Bacteria*; Blankenship, R. E., Madigan, M. J., Bauer, C. E., Eds.; Kluwer Academic Publishers: New York, 1995.
(6) van Grondelle, R.; Dekker, J. P.; Gillbro, T.; Sundström, V. *Biochim. Biophys. Acta* **1994**, *1187*, 1.
(7) Förster, T. *Naturwissenschaften* **1946**, *33*, 146. Förster, T. *Ann. Phys. (Paris)* **1948**, *2*, 55.
(8) Struve, W. S. *Fundamentals of Molecular Spectroscopy*; John Wiley & Sons: New York, 1989.
(9) Gouterman, M. In *The Porphyrins: Physical Chemistry, Part A*; Dolphin, D., Ed.; Academic Press: New York, 1978; Vol. III, Chapter 1.
(10) *Phthalocyanines: Properties and Applications*; Leznoff, C. C., Lever, A. B. P., Eds.; VCH Publishers: New York, 1989; Vol. 1−4.
(11) Wöhrle, D.; Gitzel, J.; Okura, I.; Aono, S. *J. Chem. Soc., Perkin Trans. 2* **1985**, 1171.
(12) Smith, T. D.; Livorness, J.; Taylor, H.; Pilbrow, J. R.; Sinclair, G. R. *J. Chem. Soc., Dalton Trans.* **1983**, 1391.
(13) Lefevre, D.; Porteu, F.; Balog, P.; Roulliay, M.; Zalczer, G.; Palacin, S. *Langmuir* **1993**, *9*, 150.
(14) Palacin, S.; Barraud, A. *J. Chem. Soc., Chem. Commun.* **1989**, 45.
(15) Parratt, L. G. *Phys. Rev.* **1954**, *95*, 359.
(16) Kjaer, K.; Als-Nielsen, J.; Helm, C. A.; Tippman-Krayer, P.; Möhwald, H. *J. Phys. Chem.* **1989**, *93*, 3200.
(17) Vaknin, D.; Kjaer, K.; Als-Nielsen, J.; Lösche, M. *Biophys. J.* **1991**, *59*, 1325.
(18) Gregory, B. W.; Vaknin, D.; Cotton, T. M.; Struve, W. S. *Thin Solid Films* **1996**, *284−285*, 849.
(19) Gaines, G. L. *Insoluble Monolayers at Liquid-Gas Interfaces*; Interscience: New York, 1966.
(20) Als-Nielsen, J.; Pershan, P. S. *Nucl. Instrum. Methods Phys. Res.* **1983**, *208*, 545.
(21) Vaknin, D. *Physica B: Condens. Matt.* **1996**, *221*, 152.
(22) Braslau, A.; Pershan, P. S.; Swislow, G.; Ocko, B. M.; Als-Nielsen, J. *Phys. Rev. B* **1988**, *38*, 2457.
(23) James, R. W. *Optical Principles of X-rays*; OxBow: Woodbridge, CT, 1982.
(24) Als-Nielsen, J.; Kjaer, K. In *Phase Transitions in Soft Condensed Matter*; Proc. NATO ASI Ser. B 211; Riste, T., Sherrington, D., Eds.; Plenum Press: New York, 1989; p 113.
(25) Born, M.; Wolf, E. *Principles of Optics*, 4th ed.; Pergamon Press: Oxford, U.K., 1970.
(26) In order to maintain a constant area for the footprint of the X-ray beam on the liquid surface, the slit widths of the reflectometer were opened with increasing Q_z. To account for the resulting variation in resolution, an extra first-order correction parameter σ_1 was introduced into the fitting routine, $\sigma = \sigma_0 - \sigma_1 Q_z$. The extracted surface roughness values reported herein (cf. Tables 1 and 2) correspond to σ_0. The value σ_1 was determined experimentally by using the reflectivities of the pure liquid substrates, which can be described in terms of surface roughnesses alone. Subsequently, σ_1 was fixed throughout the analyses of the spread films. It should be noted that σ_1 affects the calculated reflectivities only at Q_z values larger than 0.6 Å^{-1}. In addition, modeling with $\sigma_1 = 0$ keeps the values of the extracted parameters within the range of the calculated error bars.
(27) Lösche, M.; Piepenstock, M.; Diederich, A.; Grünewald, T.; Kjaer, K.; Vaknin, D. *Biophys. J.* **1993**, *65*, 2160.
(28) Kalyanasundaram, K. *Inorg. Chem.* **1984**, *23*, 2453.
(29) Cropek, D. M.; Bohn, P. W. *J. Phys. Chem.* **1990**, *94*, 6452.
(30) Xu, Z.; Lau, S.; Bohn, P. W. *Surf. Sci.* **1993**, *296*, 57.
(31) Ohta, N.; Matsunami, S.; Okazaki, S.; Yamazuki, I. *Langmuir* **1994**, *10*, 3909.
(32) Schick, G. A.; Schreiman, I. C.; Wagner, R. W.; Lindsey, J. S.; Bocian, D. F. *J. Am. Chem. Soc.* **1989**, *111*, 1344.
(33) Möbius, D.; Orrit, M.; Grüniger, H.; Meyer, H. *Thin Solid Films* **1985**, *132*, 41.
(34) Orrit, M.; Möbius, D.; Lehmann, U.; Meyer, H. *J. Chem. Phys.* **1986**, *85*, 4966.
(35) Claesson, P.; Carmona-Ribeiro, A. M.; Kurihara, K. *J. Phys. Chem.* **1989**, *93*, 917.
(36) Ulman, A. *An Introduction to Ultrathin Organic Films*; Academic Press: San Diego, CA, 1991.
(37) Gregory, B. W.; Vaknin, D., unpublished observations.
(38) Möhwald, H. *Rep. Prog. Phys.* **1993**, *56*, 653.
(39) Jacquemain, D.; Leveiller, F.; Weinbuch, S. P.; Lahav, M.; Leiserowitz, L.; Kjaer, K.; Als-Nielsen, J. *J. Am. Chem. Soc.* **1991**, *113*, 7684.
(40) Since the molecular area was calculated knowing both the number of molecules spread and the trough area, this latter assumption is quite reasonable given the errors associated with the 10 μL of DHDP/$CHCl_3$ syringe (graduated in 0.1 μL increments) used to spread the film and the trough area (known to <0.5%).
(41) Gregory, B. W.; Vaknin, D.; Gray, J. D.; Ocko, B. M.; Cotton, T. M.; Struve, W. S., manuscript in preparation.
(42) Harlos, K.; Eibl, H.; Pascher, I.; Sundell, S. *Chem. Phys. Lipids* **1984**, *34*, 115.
(43) Pascher, I.; Sundell, S. *Chem. Phys. Lipids* **1982**, *31*, 129.
(44) Fisch, M. J.; Trucks, G. W.; Head-Gordon, M.; Gill, P. M. W.; Wong, M. W.; Foresman, J. B.; Johnson, B. G.; Schlegel, H. B.; Robb, M. A.; Replogle, E. S.; Gomperts, R.; Andres, J. L.; Raghavachari, K.; Binkley, J. S.; Gonzalez, C.; Martin, R. L.; Fox, D. J.; Defrees, D. J.; Baker, J.; Stewart, J. J. P.; Pople, J. A. *Gaussian 92*, Revision A; Gaussian, Inc.: Pittsburgh, PA, 1992.
(45) Buchholz, J. C.; Somorjai, G. A. *J. Chem. Phys.* **1977**, *66*, 573.
(46) Bedzyk, M. J.; Bommarito, G. M.; Caffrey, M.; Penner, T. L. *Science* **1990**, *248*, 52.
(47) Wang, J.; Bedzyk, M. J.; Penner, T. L.; Caffrey, M. *Nature* **1991**, *354*, 377.

(48) Meyer, Jr., E. F.; Cullen, D. L. In *The Porphyrins*; Dolphin, D., Ed.; Academic Press: New York, 1979; Vol. III, Part A, Chapter 11.

(49) Smith, T. D.; Livorness, J.; Taylor, H.; Pilbrow, J. R.; Sinclair, G. R. *J. Chem. Soc., Dalton Trans.* **1983**, 1391.

(50) Chau, L. K.; England, C. D.; Chen, S.; Armstrong, N. R. *J. Phys. Chem.* **1993**, *97*, 2699.

(51) Birks, J. B. *Photophysics of Aromatic Molecules*; Wiley-Interscience: London, 1970.

(52) Palacin, S.; Ruaudel-Teixier, A.; Barraud, A. *J. Phys. Chem.* **1986**, *90*, 6237.

(53) Palacin, S.; Ruaudel-Teixier, A.; Barraud, A. *J. Phys. Chem.* **1989**, *93*, 7195.

(54) Schmidt, A.; Chau, L. K.; Back, A.; Armstrong, N. R. In *Phthalocyanines: Properties and Applications*; Leznoff, C. C., Lever, A. B. P., Eds.; VCH Publishers: New York, 1996; Vol. 4, Chapter 8, and references therein.

(55) Kern, R.; Le Lay, G.; Metois, J. J. In *Current Topics in Materials Science*; Kaldis, E., Ed.; North-Holland: Amsterdam, 1979; Vol. 3, Chapter 3.

(56) Chau, L. K.; Arbour, C.; Collins, G. E.; Nebesny, K. W.; Lee, P. A.; England, C. D.; Armstrong, N. R.; Parkinson, B. A. *J. Phys. Chem.* **1993**, *97*, 2690.

(57) Pasternack, R. F.; Huber, P. R.; Boyd, P.; Engasser, G.; Francesconi, L.; Gibbs, E.; Fasella, P.; Venturo, G. C.; Hinds, L. deC. *J. Am. Chem. Soc.* **1972**, *94*, 4511.

(58) Vergeldt, F. J.; Koehorst, R. B. M.; van Hoek, A.; Schaffsma, T. J. *J. Phys. Chem.* **1995**, *99*, 4397.

(59) Möhwald, H.; Miller, A.; Stich, W.; Knoll, W.; Ruaudel-Teixier, A.; Lehmann, T.; Fuhrhop, J.-H. *Thin Solid Films* **1986**, *141*, 261.

(60) Chou, H.; Chen, C.-T.; Stork, K. F.; Bohn, P. W.; Suslick, K. S. *J. Phys. Chem.* **1994**, *98*, 383.

(61) Loschek, R.; Möbius, D. *J. Chim. Phys.* **1988**, *85*, 1041.

(62) Bull, R. A.; Bulkowski, J. E. *J. Colloid Interface Sci.* **1983**, *92*, 1.

(63) Kroon, J. M.; Sudhölter, E. J. R.; Schenning, A. P. H. J.; Nolte, R. J. M. *Langmuir* **1995**, *11*, 214.

(64) Porteu, F.; Palacin, S.; Ruaudel-Teixier, A.; Barraud, A. *Makromol. Chem., Macromol. Symp.* **1991**, *46*, 37.